Generation of coherent attosecond pulses from a nano-tube array illuminated by a high-power femtosecond laser

New Journal of Physics

Generation of coherent attosecond pulses from a nano-tube array illuminated by a high-power femtosecond laser

S Y Chung[1]**, S W Hwang**[2]**, K Lee**[3]**, D Kim**[4,5,6] **and H J Lee**[2,6]

[1] Plasma Technology Research Center, National Fusion Research Institute, Daejeon 305-806, Korea
[2] Department of Electrical Engineering, Pusan National University, Busan 609-735, Korea
[3] Center for Quantum-Beam-based Radiation Research, Korea Atomic Energy Research Institute, Daejeon 305-353, Korea
[4] Department of Physics, POSTECH, Pohang 790-784, Korea
[5] Center for Attosecond Science and Technology, POSTECH, Pohang 790-784, Korea
E-mail: haejune@pusan.ac.kr and kimd@postech.ac.kr

Abstract.   A method to generate an isolated single-cycle attosecond pulse from the interaction of a high-power femtosecond laser pulse with a nano-tube array is demonstrated using a two-dimensional relativistic particle-in-cell simulation. The radiation mechanism is relativistic nonlinear Thomson scattering from the electrons in a target material. Coherent radiation is emitted in the direction of specular reflection for the incident laser pulse while the electrons make a bunch size smaller than a wavelength of the laser pulse. Maintaining the coherence of the radiation from the electrons is essential to get an intense attosecond duration, which is achieved by using a nano-tube array target and a sharply increasing laser pulse. Optimal conditions for attosecond pulse generation are investigated by parameter scanning over plasma density, target thickness and laser pulse duration.

[6] Authors to whom any correspondence should be addressed.

IOP Institute of Physics Φ DEUTSCHE PHYSIKALISCHE GESELLSCHAFT

Contents

1. Introduction

There has been significant progress in attosecond science and technology over the last decade [1–3]. Further progress would be enabled by attosecond-pump and attosecond-probe spectroscopy using an intense attosecond pulse of the order of atomic-unit-of-time (~ 24 as). Current attosecond pulses are mainly based on high-order harmonics, but it is well known that the flux and photon energy of attosecond pulses generated with the use of this technology is limited [2]. Most of the recent state-of-the-art technology of high harmonic generation (HHG) has been achieved to extend the photon energy in the soft and hard x-ray region by the introduction of mid-infrared (mid-IR) lasers [4, 5]. The emission can be phase matched simultaneously in this approach to achieve harmonic flux usable for application. For example, demonstration of bright 1.6 keV harmonics showed potential for few attosecond pulse durations at high photon energies [6] or even a zeptosecond time scale [5, 7].

Another approach to overcome the limit of photon flux is to utilize a plasma as a medium. Since a very strong field can be applied to electrons in a plasma, brighter radiation can be produced from a laser–plasma interaction. Various methods for ultra-short x-ray pulse generation using laser–plasma interactions have been proposed and demonstrated experimentally [8–12]. It was observed by a particle-in-cell (PIC) simulation that an electron nano-bunch is formed to generate coherent synchrotron radiation when a p-polarized intense short laser pulse is obliquely incident on overdense plasma [13]. Recently, a mechanism for the generation of coherent synchrotron radiation driven by the combined action of the incident laser and ionic potentials on overdense plasma slabs was reported [14]. In this paper, a quantitative theory of attosecond pulse generation was studied based on an explicit analysis of synchrotron-type electron trajectories calculated by a one-dimensional PIC simulation. With this theory, it became possible to combine the PIC simulation which includes self-consistent reactions among plasma particles with the calculation of intense extreme ultraviolet (EUV) and x-ray radiation. In this study, we extended this concept to a two-dimensional electromagentic (EM) PIC simulation combined with the calculation of far-field radiation.

It has been known that relativistic nonlinear Thomson scattering (RNTS) is a good source of attosecond radiation from the interaction of an electron nano-bunch and an ultra-intense laser pulse [15]. However, coherence of the radiation is necessary to generate high-intensity ultra-short pulses. In this study, we propose a method to generate an isolated single-cycle attosecond pulse based on RNTS produced by the interaction of a high-power femtosecond laser which is obliquely incident on an overdense plasma as shown in figure 1. Simulations have been carried out with a two-dimensional EM PIC code [16] which is combined with the calculation
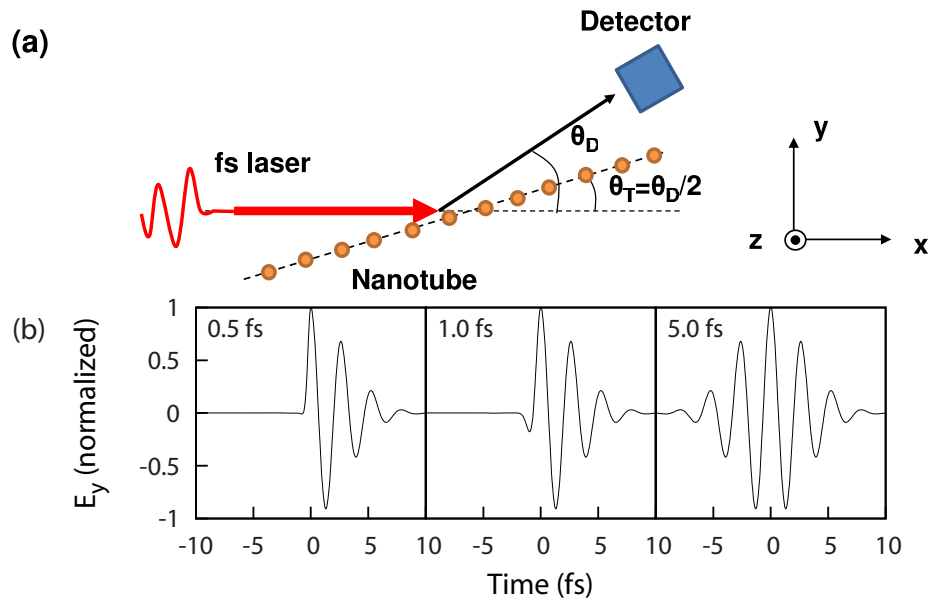
(a)

Figure 1. (a) The schematic diagram of the interaction geometry of a femtosecond laser pulse with a nano-tube array. The specular reflection coherent condition is obtained at the angles satisfying the relation $\theta_T = \theta_D/2$. (b) The p-polarized electric field described by equation (1) for different τ_1: 0.5, 1.0 and 5 fs.

of far-field radiation using the Liénard–Wiechert potential [17, 18] from the electron dynamics. This technique is more practical than the finite-difference time-domain (FDTD) methods (i.e. EM-PIC itself) [12] for short wavelength radiation (EUV or x-ray) in the far field. With this combined simulation method, it is possible to calculate the radiation from the self-consistent electron dynamics during laser–matter interaction.

This paper concentrates on the properties of an attosecond pulse generated by the RNTS of the electrons in a thin target with the variation of target shape, density, thickness and laser pulse duration. The theoretical background of the proposed RNTS scheme is explained in section 2. The considered parameter range and simulation conditions are explained in section 3. The simulation results are explained in section 4, followed by conclusions presented in section 5.

2. Theoretical background for a proposed scheme

When an electron interacts with a strong laser pulse with a normalized vector potential $a = eE/m_e c\omega_L$ greater than 1, the Lorentz factor γ of the electron becomes large, and the dynamics of the electron become nonlinear. Here, e is the charge of an electron, E is the electric field intensity of the laser, m_e is the electron mass, c is the speed of light and ω_L is the angular frequency of the laser. Such a relativistic nonlinear motion of the electron can emit x-ray pulses called RNTS [19, 20]. It was shown that a train of an attosecond x-ray pulse can be emitted from a single electron [15]. However, because many electrons are involved in actual experiments, the coherence between the radiation from each electron is an important consideration to generate an attosecond pulse using RNTS [18]. The coherence is also important to generate high-power

radiation because the radiation intensity is proportional to the square of the number of radiators (i.e. electrons) in the coherent case. Lee *et al* [21] have investigated the coherent superposition of RNTS from a group of free electrons. However, in this paper, the condition of coherent radiation is studied. To promote the coherent superposition of radiators, we propose a nano-tube array [22] adopting specular reflection condition [21] as well as a sharply increasing laser pulse [23–25]. Figure 1(a) shows a schematic diagram of the interaction geometry. When a thin film is considered as a target instead of nano-tubes, the space between nano-tubes is filled with material with a thickness d.

A condition imposed for a single attosecond pulse radiation is that all the RNTS radiations from electrons arrive at a detector at an angle θ_D (with respect to the direction of the laser propagation) within a radiation duration of the RNTS from a single electron. This condition requires that the RNTS radiation from the whole electrons inside a thin layer whose thickness (d) is less than $c\Delta t_s / \sin\theta_T$ can be coherently superposed. Here, $\theta_T = \theta_D/2$ is the angle between the nano-tube array and the laser propagation, and Δt_s is the radiation duration from a single electron. Considering this condition, the thickness of the layer should be of the order of a few to tens of nanometers. In other words, for the thickness of a thin layer d, the time interval between the radiations from the front and the back plane of the layer is $\Delta t = d\sin\theta_T/c$. If Δt is much shorter than the oscillation period of the radiation, the radiations from the target can be coherently superposed. Hence, the thinner the layer is, the higher the degree of superposition that is obtained.

However, adopting a thin layer is not sufficient because the coherence is not affected by the initial thickness of the electron layer but by the thickness at the moment of radiation. As soon as a thin layer interacts with a strong laser pulse, electrons are accelerated and are separated from ions to generate strong Coulomb force. The expansion of the layer due to Coulomb force needs to be controlled in order to enhance the degree of coherence resulting from the superposition of radiators.

3. Simulation conditions

A series of simulations were carried out to confirm the generation of attosecond pulses. A two-dimensional EM PIC code [16] was parallelized with graphic-processing units in order to increase the simulation speed and combined with radiation calculation routine. To avoid the heavy computational load encountered when using an extremely fine mesh size as necessary for a FDTD scheme, the radiated fields were calculated using the Liénard–Wiechert potential [17] from the particle motion obtained by PIC simulation as

$$\vec{E}(t') = \frac{e}{c} \left[\frac{\hat{n} \times \{(\hat{n} - \vec{\beta}) \times \dot{\vec{\beta}}\}}{(1 - \vec{\beta} \cdot \hat{n})^3 R} \right], \tag{1}$$

when t' is the retarded time, $\hat{n}$ is the unit vector of direction from the electron to the detector and R is the distance from the electron to the detector. $\dot{\vec{\beta}} = \mathrm{d}\vec{\beta}/\mathrm{d}t$ and $\vec{\beta} = \vec{v}/c$ with a particle velocity $\vec{v}$. Radiated fields from all macro particles of electrons were added in the detector's frame [18] and were converted to the actual radiation, considering the number ratio between the macro particles and actual electrons of the targets.

Figure 1(a) shows a schematic diagram of the interaction geometry of a femtosecond laser pulse with a nano-tube array. The nano-tubes are aligned in the z-direction with a length

IOP Institute of Physics   Φ DEUTSCHE PHYSIKALISCHE GESELLSCHAFT

Table 1. Parameters for the laser and target, and the simulation conditions.

Laser	Wavelength (λ)	800 nm
	Front pulse width (τ_1)	0.5–2 fs
	Rear pulse width (τ_2)	5 fs
	Peak intensity (I_0)	1×10^{20} W cm^{-2}
	Beam waist (w_0)	16 μm
Target	Electron density (n_e)	$10\,n_{cr}$
	Nano-tube diameter (d)	2.5–20 nm
	Nano-tube spacing (s)	25 nm
	Nano-tube array width (W)	4 μm
	Thin film thickness (d)	1.25–10 nm
	Thin film width (W)	4 μm
Domain	Window size (L_x, L_y)	12 μm × 48 μm
	Cell number (N_x, N_y)	2048 × 8192

comparable to the laser waist at the focal plane. The diameter of the nano-tube is 5 nm and they are aligned regularly with a period of 25 nm in the range of 4 μm. The angle between the nano-tubes array and the laser propagation direction is θ_T. The laser pulse propagates in the x-direction and is polarized in the y-direction. In the simulation, the laser is focused on the center of the nano-tube array with a beam waist of 16 μm and a laser intensity of 1.0×10^{20} W cm^{-2} ($a = 6.8$). The electron density is $10\,n_{cr}$, where n_{cr} is the critical density corresponding to the wavelength of the laser, 800 nm. The dimension of the simulation window is 12 μm on the x-axis and 48 μm on the y-axis. There are 2048 cells on the x-axis and 8192 cells on the y-axis. A moving window, which moves in the x-direction at the speed of light, is used. In all 1024 macro particles are aligned per cell. The simulation conditions are summarized in table 1.

The radiation is calculated toward the angle of θ_D which was optimized to get the highest radiation intensity. For example, the optimized θ_D is determined in the range between 11.0° and 12.0° for the τ_1 from 0.5 to 1.0 fs and $\theta_D = 25°$ for $\tau_1 = 5$ fs.

In order to minimize the detrimental effect by Coulomb force and thereby enhance the coherence, two methods addressing geometry and interaction time were proposed. Firstly, replacing a thin layer with a nano-tube array is a good solution to reduce the Coulomb force between electrons. The expansion of electrons in a cylindrical target is slower than that in a planar target, and coherence is maintained for a longer time. For this reason, we used an array of nano-tubes to minimize the Coulomb force. Therefore, the smaller size of radiation sources than that of a thin film target is maintained to enhance the coherent superposition condition.

Secondly, the interaction time of the laser with electrons can be reduced by using a sharply increasing laser pulse [23–25]. The sharply increasing laser pulse helps electrons radiate even before the significant expansion of a density profile takes place. Figure 1(b) shows the time history of a p-polarized electric field. The shape of the laser pulse is expressed as

$$E_y = E_0 \exp\left[-2\ln 2 \frac{(t - x/c)^2}{\tau^2}\right] \frac{w_0}{w} \exp\left(-\frac{y^2}{w^2}\right) \cos\left(\omega t - kx + \psi_G - \frac{kr^2}{2L}\right), \tag{2}$$

where $\tau = \tau_1$ when $t < 0$ and $\tau = \tau_2$ when $t \geqslant 0$. w_0 is the laser beam waist, $L = x[1 + (x_r/x)^2]$ and $w = \sqrt{1 + x/x_r}$ with Rayleigh length $x_r = \pi w_0^2/\lambda$. $k = 2\pi/\lambda$ is the wavenumber with the
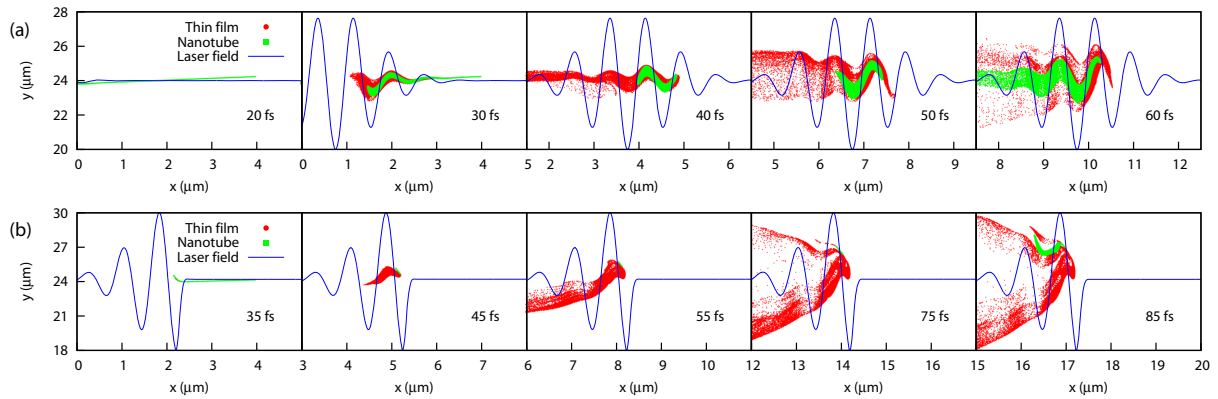
Figure 2. Time sequence of the distributions of simulated particles and the propagating laser pulse are plotted for (a) $\tau_1 = 5$ fs and (b) $\tau_1 = 0.5$ fs. Green dots are for nano-tube and red for thin film. Coherent radiation is emitted when the size of electron distribution is smaller than the wavelength of the incident laser pulse.

laser wavelength λ, and $\psi_G = \tan^{-1}(x/x_r)$ is the Gouy phase. τ_1 was varied from 0.5 to 5 fs in simulations with $\tau_2 = 5$ fs. The results show that the radiation in the front part of the pulse is much stronger than that in the rear part of the pulse because the coherence is rapidly broken after the electrons interact with the front part of the laser field and are spread by the Coulomb force.

4. Simulation results

Figure 2 shows the evolution of the electron distribution after the interaction between targets and a laser pulse with $\tau_1 = 5$ fs (figure 2(a)) and $\tau_1 = 0.5$ fs (figure 2(b)). Both the thickness of the thin film and the diameter of the nano-tube are 5 nm. As seen in figure 2, electrons from a thin film expand more quickly than those from a nano-tube array. Combining a sharply increasing laser pulse with a nano-tube array, the thickness of radiation source remains thin for a longer time than the laser pulse period. While the nano-tube array interacts with the first cycle of a sharply increasing laser pulse, the electrons are accelerated and γ increases rapidly up to several tens. The Coulomb force between electrons is effectively reduced by $1/\gamma$, which leads to the suppressed spreads of electrons especially for the nano-tube target. After the interaction with the first cycle, γ decreases to unity again and the expansion begins. The expansion makes each electron interact with different laser phases both in the laser propagation direction and in the transverse direction. When the electron motion becomes random, the radiation is not coherent any more. This is the reason for the single-cycle attosecond pulse. The radiation intensity of the second strongest pulse (produced in the second cycle) is reduced by six orders of magnitude. This leads to a single-cycle isolated attosecond.

The effect of the laser rise time (τ_1) on the magnitude of the electric field of the radiation and spectra are shown in figure 3. An isolated attosecond pulse was generated and the full-width at half-maximum of the radiation intensity was 24 as at a photon energy of 100 eV when $\tau_1 = 0.5$ fs. The radiation intensity decreases with increasing τ_1, but the changes in the pulse width and the spectrum of the radiation are relatively small when $\tau_1 \leqslant 0.8$ fs. The total radiated
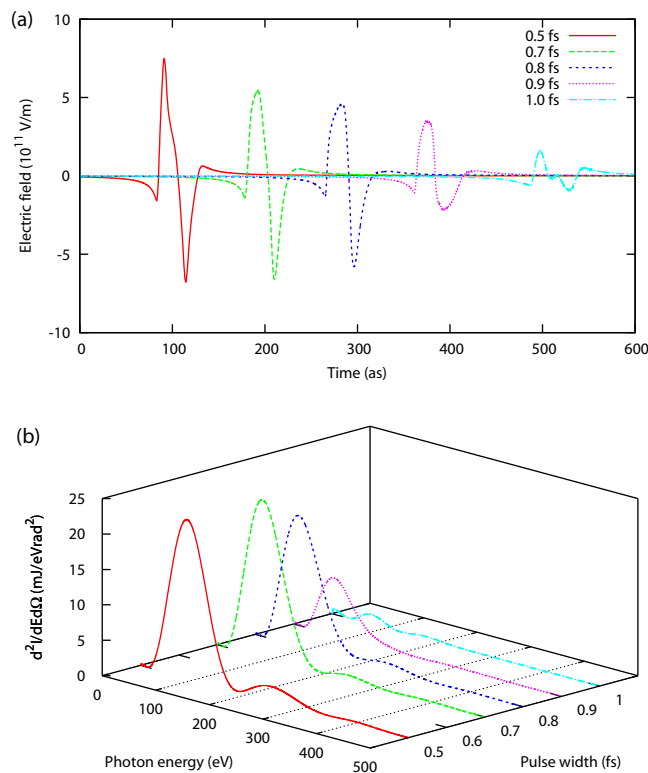
Figure 3. The increase of τ_1 results in the decrease of (a) the electric field intensities of the radiation and (b) the spectra of angular intensity at the detector position for the case of a nano-tube with a diameter of 5 nm. However, the change in the radiation spectra is relatively small if $\tau_1 \leqslant 0.8$ fs.

energy in the case of $\tau_1 = 1.0$ fs is 17.5 times smaller than that in case of $\tau_1 = 0.7$ fs. If τ_1 increases to 2.0 fs, an attosecond pulse is still generated with a pulse width of 210 as at the averaged photon energy of 60 eV. However, the radiated energy is about 1000 times smaller than that in case of $\tau_1 = 0.7$ fs. The peak angular intensity and peak spectral angular energy are 6.5×10^{16} W rad^{-2} and 8.9 mJ eV^{-1} rad^{-2}, respectively. When the detector covers the angular cross section of 1 μrad^2, the peak power is 65 GW and the total pulse energy is 1.84 μJ. Since the used laser pulse energy is about 1.0 J, this corresponds to an efficiency of 1.84×10^{-6}.

Figure 4 shows the magnitude of the electric fields of the radiation and the spectra for the variation of nano-tube diameter (figure 4(a)) and thin film thickness (figure 4(b)). Note that a single-cycle or a sub-cycle attosecond pulse is generated. After the bunch of electrons interact with the first cycle of the laser pulse, expansion occurs and the initial coherence condition starts to be broken. The superposition of all the radiation leads to a single-cycle or a sub-cycle attosecond pulse, depending on the initial size of the target and expansion speed. In the specific range of the expansion speed, the electron bunch thickness satisfies the coherent condition only while it radiates the first cycle of the pulse but does not for the second cycle. Then, it radiates a half-cycle pulse because the coherent first cycle radiation is much stronger than that of the incoherent second cycle. It means that the shape of the emitted pulse can be changed from a single-cycle to a sub-cycle pulse with the control of the expansion speed and the target thickness. As shown in figure 4(a), the radiation is a single-cycle pulse for a nano-tube array target of 5 nm
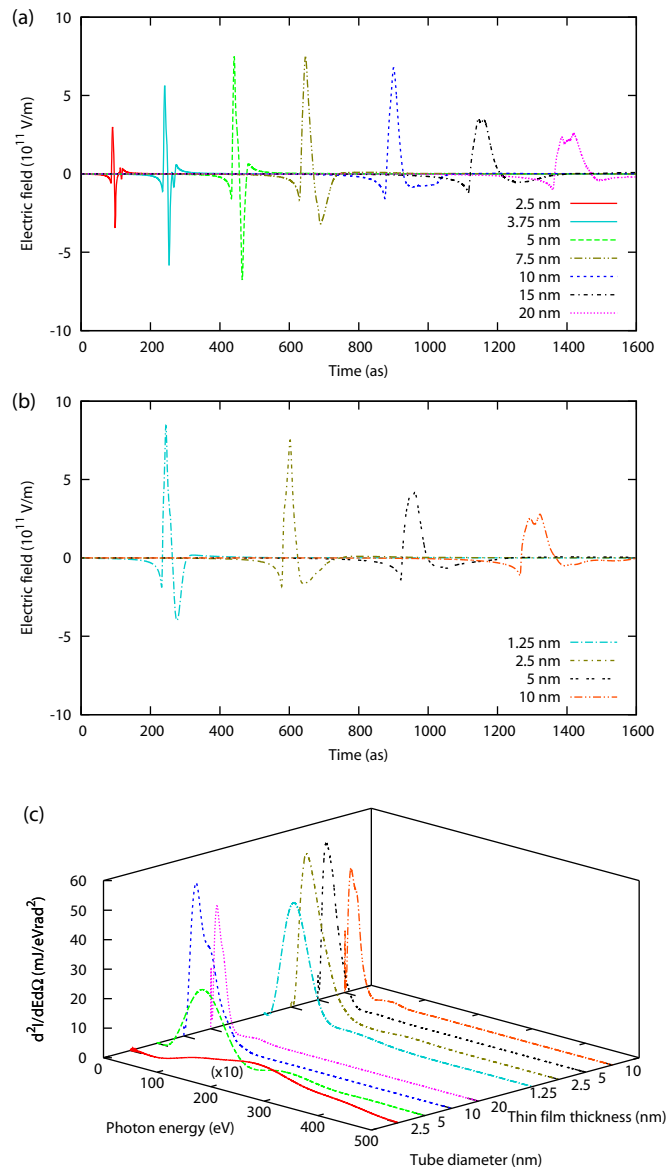
Figure 4. The radiating electric field intensities calculated for the variation of (a) nano-tube diameter and (b) thin film thickness show the change of pulse shape and (c) the spectra of angular intensity at the detector position with $\tau_1 = 0.5$ fs. The spectrum with a tube thickness of 2.5 nm is magnified by a factor of 10.

diameter and a sub-cycle pulse for a 20 nm diameter. The change of the pulse shape is also observed for the thin film target in figure 4(b), but the necessary target size for a single-cycle pulse is much smaller in case of a thin film than in the case of a nano-tube array.

In both cases of nano-tubes and thin films, the radiation pulse duration increases with increasing target size. However, there is an optimal condition for the radiation intensity. As shown in figure 4(c), the radiation intensity in case of a 2.5 nm nano-tube is lower than that of a 5 nm nano-tube case because the total number of electrons interacting with the laser is smaller in case of the 2.5 nm nano-tube array. The spectral peak intensity in case of the 2.5 nm
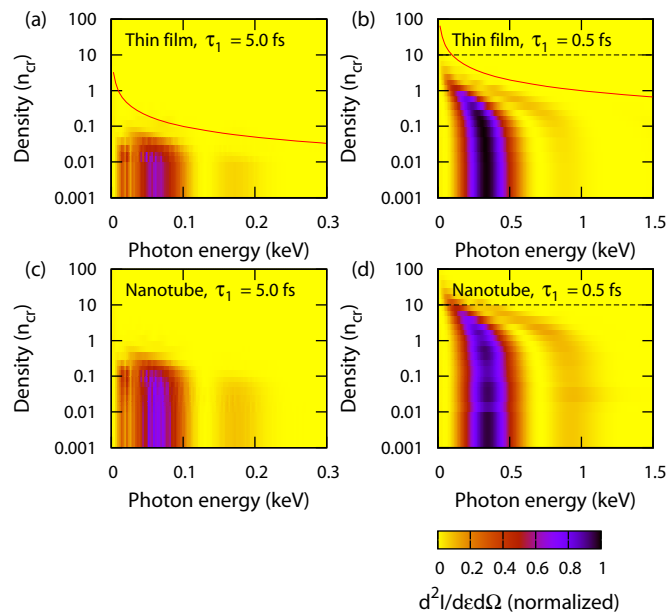
Figure 5. The contour plot of spectra with respect to the target density for different target types ((a), (b) thin film and (c), (d) nano-tube array) and for different rising time of the laser pulse ((a), (c) $\tau_1 = 5.0$ fs and (b), (d) $\tau_1 = 0.5$ fs). Coherence is maintained for a density higher than $10\,n_{cr}$ (dashed line) for case (d).

nano-tube around 300 eV is about 16 times smaller than that in case of the 5 nm nano-tube. If the diameter becomes larger than 10 nm, the coherence is more easily broken with a smaller peak intensity and photon energy, which leads to a sub-cycle pulse period. Thin film cases show the same trend, but the necessary thickness is much smaller for an isolated single-cycle pulse, and photon energy is normally less than 100 eV.

The condition for the coherence of the radiation at a given wavelength is controlled by the size of the radiation source which is determined by electron density as well as the initial target size. The investigation for the effect of plasma density on the spectra with the variation of the target shape (thin film versus nano-tube) and the laser rising time ($\tau_1 = 5$ versus 0.5 fs) is summarized in figure 5. All the spectra in each color map were calculated from the same number of macro particles and normalized by the peak value of four graphs.

For the coherent superposition of a wavelength at a detector, the size of the radiation source should be several times smaller than the wavelength. This is satisfied more easily in a longer wavelength region. The lower limit of the coherence for a wavelength is proportional to the size of the radiation source. Because the size of the radiation source is proportional to the Coulomb field, the coherence limit for a wavelength is proportional to the density (i.e. the lower limit for coherence in terms of the photon energy is inversely proportional to the density). The red solid lines in figures 5(a) and (b) show this relation well, indicating that the coherence is governed by the Coulomb field for thin film targets. As the density increases, the coherence becomes worse and the radiation becomes weaker rapidly from the region of higher photon energy. The coherence in the case of a nano-tube array is still kept for about one order of magnitude higher density than in the case of thin film ((a) versus (c) and (b) versus (d)). The effect of the rapidly increasing pulse shape with a short τ_1 is also significant ((a) versus (b) and (c) versus (d)).
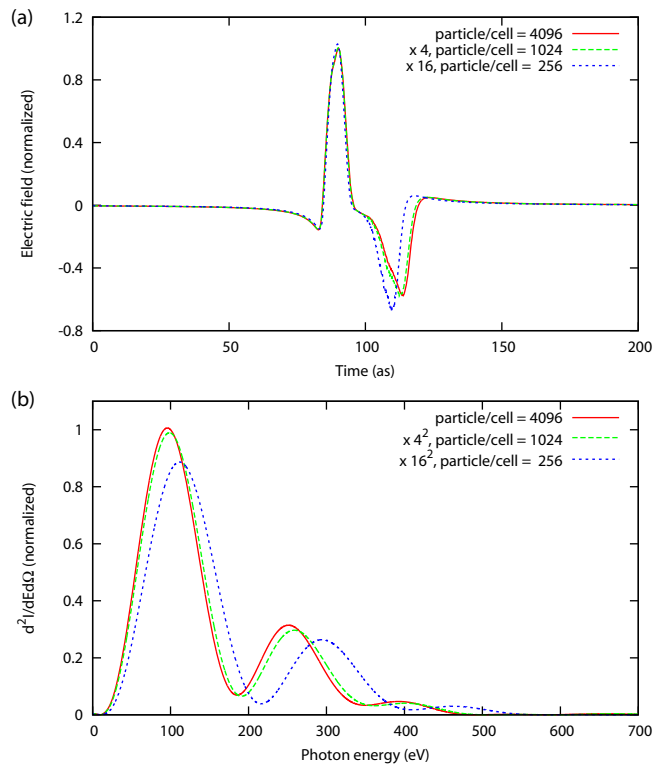
Figure 6. The comparison of the effect of different simulation particle numbers per cell, N_c, is shown on (a) the time history of electric fields and (b) the spectrum of the radiation for $N_c = 4096$, 1024 and 256. These quantities increase quadratically with the increase of N_c.

The coherence is maintained even in ten times higher density as the temporal shape of the laser pulse changes from a normal Gaussian pulse ($\tau_1 = 5$ fs) to a sharply increasing pulse ($\tau_1 = 0.5$ fs). For a nano-tube array with a sharply increasing laser pulse, the coherence is still kept even for a 100 times higher density than that for a thin film with a normal Gaussian laser pulse. The coherence maintained at high electron density is essential because a lower density ($\lesssim 10 \, n_{cr}$) is not available for real experiments. In figure 5(d), we note that the coherence is maintained for a density higher than $10 \, n_{cr}$ which is of the order of 10^{22} cm^{-3} and close to a solid density. The results imply that real experiments can be performed with normal materials.

The radiation from each electron can be added constructively, destructively or randomly at a different temporal or spectral region. The coherence was checked by changing the number of macro particles per cell from 256 to 4096 as shown in figure 6. Coherence condition is satisfied as the radiation intensity increases by a factor of 4^2 with the increase of N_c by a factor of 4 from 1024 to 4096. It is marginally satisfied for $N_c = 256$, but there exists almost 10% of errors from the noise of sparse particle distributions.

The incoherent part (e.g., photon energy > 2 keV in this study) is smaller by five orders of magnitude than the strongest (coherent) part. In spite of a two-dimensional simulation, the effect of the laser spot size varying in the z-direction was also taken into account in the results because a series of simulations were carried out for the various laser intensities in the range of $-5 < z < 5 \, \mu$m.

IOP Institute of Physics ⬧ DEUTSCHE PHYSIKALISCHE GESELLSCHAFT

5. Conclusions

A series of two-dimensional PIC simulations combined with the Liénard–Wiechert potential for radiation showed that isolated single-cycle or sub-cycle attosecond pulses can be generated by RNTS from the interaction of a strong laser pulse with a thin target. To get a strong attosecond pulse, a strong coherence of the RNTS from electrons is essential. A specular reflection condition and coherent motion of electrons should be satisfied to obtain strong coherent radiation. Very strong coherent radiation is emitted in the direction of specular reflection of the incident laser pulse only when the size of the electron bunch is smaller than a wavelength of the laser pulse as shown in figure 2(b).

As the expansion of electron distribution is caused by the Coulomb force among electrons after the interaction with the laser pulse, it is possible to increase the radiation intensity by manipulating the target shape or modulating the laser pulse profile. Two options are proposed for the increase of radiation intensity with the reduction of Coulomb force between electrons. The first one is to utilize a nano-tube array instead of a thin-film target. The developed nano-technology will make it possible to manipulate a required target [22]. The second one is to utilize a sharply increasing laser pulse in order to make a very strong interaction between the electrons and the laser pulse before the electron distribution expands to be larger than the wavelength of the laser pulse. The developed plasma mirror technique [23, 25] will make it possible to achieve a very rapidly rising pulse.

A nano-tube array along with a sharply increasing laser pulse is shown to satisfy the condition for coherent superposition even with a plasma density of $10\,n_{cr}$. The efficiency is similar to that of the generation of an attosecond pulse using HHG [26, 27], and a higher photon energy can be achieved by increasing the driving laser energy. Therefore, the suggested method is a good candidate to generate an intense and isolated single-cycle or a sub-cycle attosecond pulse. The prepulse effect has not been discussed much in this study and requires more work. However, this problem could be overcome with the improvement of the plasma mirror technique for high intensity short laser pulses and a tightly focused RNTS technique [28] which will be treated in the future work. In addition, if high-intensity mid-IR lasers are utilized as a driver in a similar way to the high-energy HHG technique [5], the limitation for the target thickness and laser rising time will be released. This is also a topic for future study.

Acknowledgments

References

[1] Corkum P B and Krausz F 2007 *Nature Phys.* **3** 381
[2] Krausz F and Ivanov M 2009 *Rev. Mod. Phys.* **81** 163
[3] Nisoli M and Sansone S 2009 *Prog. Quantum Electron.* **33** 17
[4] Popmintchev T, Chen M-C, Bahabad A, Gerrity M, Sidorenko P, Cohen O, Christov I P, Murnane M M and Kapteyn H C 2009 *Proc. Natl Acad. Sci. USA* **106** 10516

IOP Institute of Physics ⦿ DEUTSCHE PHYSIKALISCHE GESELLSCHAFT

[5] Popmintchev T, Chen M-C, Arpin P, Murnane M M and Kapteyn H C 2010 *Nature Photon.* **4** 822

[6] Popmintchev T *et al* 2012 *Science* **336** 1287

[7] Hernández-García C, Pérez-Hernández J A, Popmintchev T, Murnane M M, Kapteyn H C, Jaron-Becker A, Becker A and Plaja L 2013 *Phys. Rev. Lett.* **111** 033002

[8] Rousse A *et al* 2004 *Phys. Rev. Lett.* **93** 135005

[9] Phuoc K T *et al* 2007 *Phys. Plasmas* **14** 080701

[10] Tsakiris G D, Eidmann K, Meyer-ter-Vehn J and Krausz F 2006 *New J. Phys.* **8** 19

[11] Pirozhkov A S, Bulanov S V, Esirkepov T Z, Mori M, Sagisaka A and Daido H 2006 *Phys. Plasmas* **13** 013107

[12] ander Brügge D and Pukhov A 2007 *Phys. Plasmas* **14** 093104

[13] an der Brügge D and Pukhov A 2010 *Phys. Plasmas* **17** 033110

[14] Mikhailova J M, Fedorov M V, Karpowicz N, Gibbon P, Platonenko V T, Zheltikov A M and Krausz F 2012 *Phys. Rev. Lett.* **109** 245005

[15] Lee K, Cha Y H, Shin M S, Kim B H and Kim D 2003 *Phys. Rev.* E **67** 026502

[16] Hwang S W, Lee H J, Chung S Y and Kim D 2010 *J. Korean. Phys. Soc.* **56** 309

[17] Jackson J D 1999 *Classical Electrodynamics* (New York: Wiley) chapter 14

[18] Chung S Y, Lee H J, Lee K and Kim D 2011 *Phys. Rev. Spec. Top.—Accelerators Beams* **14** 060705

[19] Esarey E, Ride S K and Sprangle P 1993 *Phys. Rev.* E **48** 3003

[20] Lee K, Cha Y H, Shin M S, Kim B H and Kim D 2003 *Opt. Express* **11** 309–16

[21] Lee K, Kim B H and Kim D D 2005 *Phys. Plasmas* **12** 043107

[22] Ding L, Tselev A, Wang J, Yuan D, Chu H, McNicholas T P, Li Y and Liu J 2009 *Nano Lett.* **9** 800

[23] Ji L, Shen B F, Zhang X M, Wang F C, Jin Z Y, Xia C Q, Wen M, Wang W P, Xu J C and Yu M Y 2009 *Phys. Rev. Lett.* **103** 215005

[24] Ji L, Shen B, Zhang X, Wen M, Xia C, Wang W, Xu J, Yu Y, Yu M and Xu Z 2011 *Phys. Plasmas* **18** 083104

[25] Wirth A *et al* 2011 *Science* **334** 195

[26] Ferrari F, Calegari F, Lucchini M, Vozzi C, Stagira S, Sansone G and Nisoli M 2010 *Nature Photon.* **4** 875

[27] Schultze M, Goulielmakis E, Uiberacker M, Hofstetter M, Kim J, Kim D F, Krausz F and Kleineberg U 2007 *New J. Phys.* **49** 243

[28] Lan P, Lu P and Cao W 2006 *Phys. Plasmas* **13** 013106